J. Fluid Mech. (2014), *vol.* 752, *pp.* 66–89.
doi:10.1017/jfm.2014.321

Dynamics of liquid films on vertical fibres in a radial electric field

Zijing Ding[1,†], Jinlong Xie[1], Teck Neng Wong[1,†] and Rong Liu[2]

[1]School of Mechanical and Aerospace Engineering, Nanyang Technological University, 639798, Republic of Singapore

[2]Institute of Mechanics, Chinese Academy of Sciences, Beijing 100190, China

(Received 9 October 2013; revised 21 March 2014; accepted 31 May 2014; first published online 2 July 2014)

The long-wave behaviour of perfectly conducting liquid films flowing down a vertical fibre in a radial electric field was investigated by an asymptotic model. The validity of the asymptotic model was verified by the fully linearized problem, which showed that results were in good agreement in the long-wave region. The linear stability analysis indicated that, when the ratio (the radius of the outer cylindrical electrode over the radius of the liquid film) $\beta < e$, the electric field enhanced the long-wave instability; when $\beta > e$, the electric field impeded the long-wave instability; when $\beta = e$, the electric field did not affect the long-wave instability. The nonlinear evolution study of the asymptotic model compared well with the linear theory when $\beta < e$. However, when $\beta = e$, the nonlinear evolution study showed that the electric field enhanced the instability which may cause the interface to become singular. When $\beta > e$, the nonlinear evolution studies showed that the influence of the electric field on the nonlinear behaviour of the interface was complex. The electric field either enhanced or impeded the interfacial instability. In addition, an interesting phenomenon was observed by the nonlinear evolution study that the electric field may cause an oscillation in the amplitude of permanent waves when $\beta \geqslant e$. Further study on steady travelling waves was conducted to reveal the influence of electric field on the wave speed. Results showed that the electric field either increased or decreased the wave speed as well as the wave amplitude and flow rate. In some situations, the wave speed may increase/decrease while its amplitude decreased/increased as the strength of the external electric field increased.

Key words: interfacial flows (free surface), MHD and electrohydrodynamics, nonlinear instability

1. Introduction

The study of thin liquid films falling down a vertical cylinder is of great importance in industrial applications, such as in coating flows, oil recovery and biological flows. The coating of fibres has received much attention, particularly in connection with the drawing of fibres from liquid baths (Quéré 1999). Experimental studies have shown that, the flow of a thin liquid film down a vertical cylinder is not stable. The surface-

† Email addresses for correspondence: mtnwong@ntu.edu.sg, zding001@e.ntu.edu.sg

tension-driven flow modulated by gravity may lead the film to breakup or evolve to finite-amplitude permanent waves (Quéré 1990; De Ryck & Quéré 1996; Zuccher 2008; Duprat, Ruyer-Quil & Giorgiutti-Dauphiné 2009).

The pioneering work of theoretical modelling of a liquid layer resting on the exterior of a cylinder was established by Goren (1962), who investigated the influences of surface tension and the ratio between liquid thickness and the radius of the solid substrate on the capillary instability via a standard linear stability analysis. Lin & Liu (1975) followed the work of Goren (1962) and studied the instability of a thin liquid film falling down the outer or inner surface of a vertical cylinder under the influence of gravity. Their results indicated that the surface tension was essentially destabilizing (Lin & Liu 1975).

In previous studies, most of the modelling work of an annular film flow has mainly focused on the use of a lubrication approximation wherein the fibre radius is considered to be much larger than the film thickness. In general, we classify these models into two groups: a Benney-type model and a two-equation model. The Benney-type model is a single asymptotic equation describing the motion of the liquid interface; while the two-equation model solves two coupling equations of the interfacial kinematic condition with one more equation governing the local flow rate. The Benney-type model was used by Frenkel (1992) to investigate an ultra thin liquid film driven by gravity down a vertical cylinder. Lister *et al.* (2006) used the Benney-type model and investigated the drainage of a liquid film on a horizontal cylinder, in which the influence of gravity was neglected. They found that it took an infinitely long time for the liquid film to rupture (Lister *et al.* 2006).

However, the Benney-type model is only valid for small flow rate problems. For a liquid film flowing down an inclined plate, it usually blows up and gives non-physical solutions when the flow rate is high (Pumir, Manneville & Pomeau 1983). The two-equation model was developed to address the drawback of the Benney-type model. Trifonov (1992) employed an integral boundary-layer model and investigated steady travelling waves in the annular viscous liquid film flow. Trifonov (1992) applied the bifurcation theory and investigated different kinds of wave families in such a flow system. Sisoev *et al.* (2006) revisited the linear and nonlinear stability of the problem (Trifonov 1992) via the integral boundary-layer model. Direct simulation of the integral boundary-layer model was performed so as to simulate the evolution of interfacial waves from the upstream to downstream (Sisoev *et al.* 2006). Later, the integral boundary-layer model was used by Shkadov, Beloglazkin & Gerasimov (2008) to investigate the solitary wave families. Notably, the integral boundary model was more accurate than the Benney-type model in predicting the linear stability when the Reynolds number was high (Sisoev *et al.* 2006), yet it fails to predict the critical Reynolds number of a thin liquid film falling down a moderately tilted plane. Ruyer-Quil & Manneville (1998) were motivated to develop a weighted-residual model which overcomes the inaccuracy of the integral boundary-layer model successfully. Ruyer-Quil *et al.* (2008) utilized the weighted-residual model to investigate the dynamics of thin liquid films flowing down a vertical cylinder. Recently, Ruyer-Quil & Kalliadasis (2012) extended their study (Ruyer-Quil *et al.* 2008) to investigate nonlinear waves in the viscous annular film.

Unlike these studies (Frenkel 1992; Trifonov 1992; Lister *et al.* 2006; Sisoev *et al.* 2006; Ruyer-Quil *et al.* 2008; Shkadov *et al.* 2008; Ruyer-Quil & Kalliadasis 2012), in which the film thickness were assumed to be much smaller than the cylinder radius, Kliakhandler, Davis & Bankhoff (2001) considered a relatively thicker liquid film down a thin vertical fibre. Three typical flow regimes (regimes ‘a’, ‘b’ and ‘c’) were

observed by Kliakhandler *et al.* (2001) in experiments (see figure 1 in Kliakhandler *et al.*'s paper). Kliakhandler *et al.* (2001) proposed a model equation to describe the motion of the liquid interface. Hereafter, we call the model of Kliakhandler *et al.* (2001) the KDB model. The KDB model retains the full curvature of the interface under the consideration of large deformation of the interface. The linear stability analysis of the KDB model compares well with the fully linearized Navier–Stokes equations, demonstrating that the model is reasonable. Nevertheless, their model failed to find the solution similar to that of flow regime 'a' (Kliakhandler *et al.* 2001). Craster & Matar (2006) revisited the problem (Kliakhandler *et al.* 2001) and used an asymptotic model. Although the linear stability analysis did not agree well with the results of the fully linearized Stokes flow when the radius of the fibre was very small, the non-trivial travelling wave solutions of the asymptotic model was in excellent agreement with the experimental observation (Craster & Matar 2006). In particular, the travelling wave solution (Craster & Matar 2006) compares quite well with the experimental observation of flow regime 'a'. The most distinct difference between the KDB model and Craster and Matar's model is that Craster & Matar (2006) simplified the interfacial curvature asymptotically and introduced an additional parameter in the Benney-type equation which was identified with the Bond number.

When a perfectly conducting liquid film falls down a vertical cylinder in the presence of an external electric field, how it responses when its interface is perturbed is in question. In fact, in previous studies, researchers focused on the electric field's influence on the dynamics of liquid jets. The breakup of an electrified liquid jet is of particular interest in academic study and industrial applications, such as ink jetting and drug delivery. The study of electric field's influence on the breakup of charged liquid jets was firstly investigated by Basset (1894). However, Basset's analysis did not agree with experimental observation. Taylor (1969) corrected the error in the analysis of Basset (1894). Saville (1971) revisited the linear stability of charged viscous cylinders by considering non-axisymmetric disturbances. He concluded that the non-axisymmetric unstable mode dominated the instability when the electric field's strength was strong. This conclusion was verified experimentally by Son & Ohba (1998). Collins, Harris & Basaran (2007) revisited the problem (Saville 1971) and investigated the nonlinear dynamics of the liquid jet. Instead of considering the non-axisymmetric problem, they considered the axisymmetric case and derived a one-dimensional model to study the linear stability and nonlinear breakup of the conducting jet. Perfectly conducting liquid jets and threads surrounded by dielectric gases or dielectric liquids in the presence of a radial electric field were investigated by Wang *et al.* (Wang, Mählmann & Papageorgiou 2009; Wang & Papageorgiou 2011). They proposed an asymptotic model under the long-wave approximation and investigated the electrostatic pressure's effect on the linear and nonlinear behaviour of the liquid jet/thread (Wang *et al.* 2009; Wang & Papageorgiou 2011). To capture the breakup of the liquid jet/thread in the vicinity of the singular event, they conducted a study by searching for self-similar solutions (Wang *et al.* 2009; Wang & Papageorgiou 2011). In these previous studies (Basset 1894; Taylor 1969; Saville 1971; Son & Ohba 1998; Collins *et al.* 2007; Wang *et al.* 2009; Wang & Papageorgiou 2011), the electrostatics was considered. Conroy *et al.* (2011) examined the influence of an AC electric field on the linear and nonlinear dynamics of a perfectly conducting liquid thread. However, the study was restricted in the framework of electrostatics provided that the frequency of the AC field was not too high. Some other researchers investigated poorly conducting liquid jets in radial electric fields. The interfacial charge transport was found to affect the linear and nonlinear dynamics

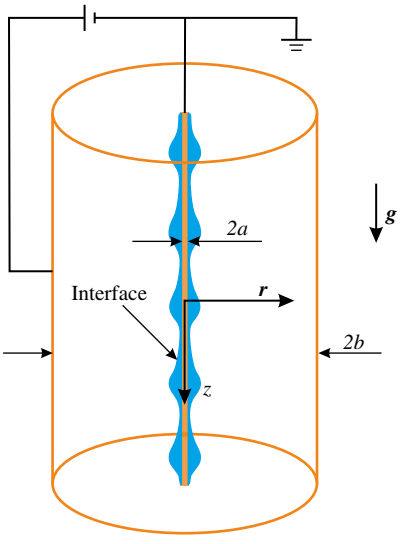

FIGURE 1. (Colour online) Geometry of the system.

of the jet profoundly (López-Herrera, Riesco-Chueca & Gañón-Calvo 2005; Wang 2012). Recently, Wray, Matar & Papageorgiou (2012) investigated a dielectric liquid film flowing down a vertical cylinder surrounded by a dielectric gas. A Benney-type model was derived so as to reveal the electric field's influence on the interfacial instability and nonlinear evolution (Wray *et al.* 2012). In their paper, it was reported that the normal Maxwell stresses destabilized the flow, whereas the tangential stresses can be either stabilizing or destabilizing.

In this paper, the influence of an electrostatic field on the dynamics of a perfectly conducting liquid film flowing down a vertical metal fibre is investigated. The rest of this paper is organized as follows. In § 2, the mathematical formulation is established. Scalings and modelling of an asymptotic model are presented in § 3. Section 4 provides the linear stability analysis of the flow and the influence of the electric field is discussed. Transient simulation of the asymptotic model is presented in § 5. The influence of the electric field on steady travelling waves are investigated in § 6. Conclusions are marked in § 7.

2. Mathematical formulation

A perfectly conducting Newtonian liquid film flowing down a vertical fibre is shown in figure 1. The annular flow system is enclosed in a coaxial cylindrical electrode. A high voltage is applied at the outer electrode, while the metal fibre is grounded. Liquids that flow down the fibre under gravity are surrounded by a dielectric gas. The radii of the fibre and electrode are $r = a$ and $r = b$, respectively.

In this paper, the axisymmetric problem is considered. The cylindrical coordinates (r, z) are chosen. The motion of liquids is governed by the continuity equation and the momentum equation:

$$\nabla \cdot \boldsymbol{u} = 0, \tag{2.1}$$

$$\rho \frac{\mathrm{D}\boldsymbol{u}}{\mathrm{D}t} = -\nabla p + \mu \nabla^2 \boldsymbol{u} + \rho \boldsymbol{g}, \tag{2.2}$$

where $\boldsymbol{u} = u\boldsymbol{e}_r + w\boldsymbol{e}_z$ is the velocity. Here $\mathrm{D}/\mathrm{D}t = \partial/\partial t + u(\partial/\partial r) + w(\partial/\partial z)$ is the material derivative operator. Here ρ is the density of the liquid and μ is the dynamical viscosity. Here $\boldsymbol{g}$ denotes the gravitational acceleration. The surrounding dielectric gas is assumed to be inviscid whose dynamics is neglected in this paper.

Since we are considering the electrostatics, the electrical potential ϕ in the dielectric gas follows the solution of Laplace's equation:

$$\nabla^2\phi = 0. \tag{2.3}$$

On the surface of the fibre $r = a$, there are no-slip and no-penetration conditions,

$$u = w = 0. \tag{2.4}$$

Since the electrical potential at the interface $r = a + h(z, t)$ is equipotential under the assumption of perfectly conducting liquids, therefore

$$\phi = 0. \tag{2.5}$$

A high electrical potential is imposed at the outer electrode,

$$\phi = \phi_0. \tag{2.6}$$

At the liquid ring's interface $r = a + h(z, t)$, the stress balance condition is expressed as

$$(\boldsymbol{T}_l - \boldsymbol{T}_g) \cdot \boldsymbol{n} = -\gamma(\nabla \cdot \boldsymbol{n})\boldsymbol{n}, \tag{2.7}$$

where $\boldsymbol{T}_l$ or $\boldsymbol{T}_g$ is the stress tensor in the liquid phase and gas phase respectively, and $\boldsymbol{T}_i = -p_i\boldsymbol{I} + \boldsymbol{T}_i^v + \boldsymbol{T}_i^M$ $(i = l, g)$. Here p_i $(i = l, g)$ represents the pressure in the liquid or gas phase. Here $\boldsymbol{T}^v = \mu[\nabla\boldsymbol{u} + (\nabla\boldsymbol{u})^{\mathrm{T}}]$ is the Newtonian stress tensor which is zero in the gas phase. In the liquid phase, the Maxwell stress is absent under the assumption of a perfectly conducting liquid film. In the gas phase, because the electrostatics is considered, the Maxwell stress $\boldsymbol{T}^M = \varepsilon[\boldsymbol{E}\boldsymbol{E} - (1/2)(\boldsymbol{E} \cdot \boldsymbol{E})\boldsymbol{I}]$. Here $\boldsymbol{I}$ is the identity tensor and ε is the electrical permittivity of the gas. Here γ represents the surface tension. Here $\boldsymbol{n}$ denotes the surface normal.

Finally, the system is closed by the kinematic condition of interface,

$$h_t + wh_z = u. \tag{2.8}$$

3. Scaling and the asymptotic model

The aim is to solve the above (2.1)–(2.8) in the long-wavelength limit. We assume that the radius of the fluid ring $\mathscr{R} = a + h_0$ (h_0 is the initial thickness of the liquid) is much smaller than its characteristic length $\mathscr{L}$ in the axial direction. Craster & Matar (2006) took the length scale $\mathscr{L}$ to be related to the capillary length: $\mathscr{L} = \gamma/\rho g\mathscr{R}$, so that the dimensionless equations would not rely on the fluid thickness being small relative to the fibre radius, but small relative to a dynamic length scale. Equations (2.1)–(2.8) are non-dimensionalized by adopting the following scales: $r = \mathscr{R}r'$, $z = \mathscr{L}z'$, $p - p_g = \rho g\mathscr{L}p'$, $\phi = \phi_0$, $w = Ww'$, $u = \epsilon Wu'$, $t = \mathscr{L}/Wt'$ where $W = \rho\mathscr{R}^2 g/\mu$ is the velocity scale and $\epsilon = \mathscr{R}/\mathscr{L}$.

After dropping the primes of the dimensionless variables, the dimensionless forms of the governing equations (2.1)–(2.3) become

$$r^{-1}(ru)_r + w_z = 0, \tag{3.1}$$

$$\epsilon^4 Re\frac{\mathrm{D}u}{\mathrm{D}t} = -p_r + \epsilon^2\left(u_{rr} + \epsilon^2 u_{zz} + \frac{1}{r}u_r - \frac{u}{r^2}\right), \tag{3.2}$$

$$\epsilon^2 Re\frac{\mathrm{D}w}{\mathrm{D}t} = 1 - p_z + \left(w_{rr} + \epsilon^2 w_{zz} + \frac{1}{r}w_r\right), \tag{3.3}$$

$$\phi_{rr} + \frac{1}{r}\phi_r + \epsilon^2\phi_{zz} = 0, \tag{3.4}$$

where $Re = (\rho W\mathscr{L})/\mu$ is the Reynolds number. Here, we follow the work of Wang *et al.* (2009) and assume that the gap between the liquid interface and the outer electrode is much smaller than the characteristic length $\mathscr{L}$.

The dimensionless boundary conditions at $r = \alpha$ are

$$u = w = 0. \tag{3.5}$$

The dimensionless radius is $\alpha = a/\mathscr{R} < 1$. When α is small, the liquid layer is relatively thicker than the fibre. When $a \to 1$, the liquid film is thin compared with the fibre radius.

At the interface $r = \alpha + h(z, t)$, the dimensionless stress balance conditions are

$$(\epsilon^2 u_z + w_r)(1 - \epsilon^2 h_z^2) + 2\epsilon^2 h_z(u_r - w_z) = 0, \tag{3.6}$$

$$-p - \frac{2\epsilon^2[(w_r + \epsilon^2 u_z)h_z - u_r - \epsilon^2 w_z h_z^2]}{1 + \epsilon^2 h_z^2} - \frac{\epsilon\mathscr{E}\left[\frac{1}{2}(\phi_r^2 - \epsilon^2\phi_z^2)(1 - \epsilon^2 h_z^2) - 2\epsilon^2\phi_r\phi_z h_z\right]}{1 + \epsilon^2 h_z^2} = \epsilon(2H\mathscr{S}), \tag{3.7}$$

in which

$$2H = -\frac{1}{(h + \alpha)(1 + \epsilon^2 h_z^2)^{1/2}} + \frac{\epsilon^2 h_{zz}}{(1 + \epsilon^2 h_z^2)^{3/2}} \tag{3.8}$$

is the curvature. Here $\mathscr{E} = \varepsilon(\phi_0)^2/\rho g\mathscr{R}^3$ is the electrical Weber number. Here $\mathscr{S} = \gamma/\rho g\mathscr{R}^2$ is the dimensionless surface tension. Here $\mathscr{E}$ is assumed to have an order of $O(\epsilon^{-1})$. The dimensionless surface tension number $\mathscr{S}$ can be connected to a Bond number $Bo = 1/\mathscr{S} = \rho g\mathscr{R}^2/\gamma$. The Bond number $Bo = \mathscr{R}/\mathscr{L} = \epsilon$ naturally measures the ratio of length scales. In experiments, Bo is typically small ($\sim$0.3 or so) (Craster & Matar 2006). We follow the work of Craster & Matar (2006) and fix the dimensionless surface tension at $\mathscr{S} = \epsilon^{-1}$ in the following discussions.

For the electric field, the boundary conditions are

$$\phi|_{r=\alpha+h(z,t)} = 0, \quad \phi|_{r=\beta} = 1. \tag{3.9a,b}$$

The dimensionless radius $\beta = b/\mathscr{R} > 1$. When $\beta \gg 1$, the outer electrode is moved far way from the liquid film.

The dimensionless kinetic condition of the free interface is written in the conservative form,

$$h_t + \frac{1}{\alpha + h}\left(\int_\alpha^{\alpha+h} rw\,\mathrm{d}r\right)_z = 0. \tag{3.10}$$

For the leading-order problem of ϵ, the flow profile is described by

$$1 - p_z + w_{rr} + \frac{1}{r}w_r = 0, \tag{3.11}$$

$$w|_{r=\alpha} = 0, \quad w_r|_{r=\alpha+h(z,t)} = 0. \tag{3.12a,b}$$

Therefore, the velocity profile yields

$$w = \frac{p_z - 1}{4}[(r^2 - \alpha^2) - 2(\alpha + h)^2 \ln(r/\alpha)]. \tag{3.13}$$

Moreover, the normal stress balance condition is reduced as

$$p = -\frac{E_b}{2}\phi_r^2 + \frac{1}{\alpha + h} - \epsilon^2 h_{zz}, \tag{3.14}$$

where ϵ is absorbed into E_b, i.e. $E_b = \epsilon\mathscr{E}$. Now, the modified dimensionless electrical Weber number E_b is assumed to be $O(1)$. The simplification of the curvature in (3.14) is suggested by Craster & Matar (2006). Inclusion of the term h_{zz} is reflected by the linear stability analysis which is vital to ensure the correct high-wavenumber cutoff occurs (Craster & Matar 2006; Lister *et al.* 2006).

The leading-order governing equation of the electrical potential ϕ writes

$$\phi_{rr} + \frac{1}{r}\phi_r = 0. \tag{3.15}$$

The solution of the leading-order approximation of the electrical potential is obtained:

$$\phi = 1 - \frac{\ln(r/\beta)}{\ln[(\alpha + h)/\beta]}. \tag{3.16}$$

Therefore, in (3.14), the electrostatic force is given by $F = \phi_r^2 = (\alpha + h)^{-2}[\ln((\alpha + h)/\beta)]^{-2}$. This electrostatic force F describes the attraction between the liquid interface and the outer electrode.

Substituting the velocity w into the kinematic equation (3.10), we obtain the evolution equation of the interfacial shape $h(z, t)$,

$$h_t + (\alpha + h)^{-1} q_z = 0, \tag{3.17}$$

with

$$q = -\frac{p_z - 1}{4}\left[(\alpha + h)^4 \ln\left(\frac{\alpha + h}{\alpha}\right) - \frac{h(2\alpha + h)(2\alpha^2 + 6\alpha h + 3h^2)}{4}\right]. \tag{3.18}$$

The pressure gradient p_z can be calculated by differentiating equation (3.14) with respect to z. Turning off the electric field, we recover the evolution equation of Craster & Matar (2006).

4. Linear stability analysis

The initial unperturbed state of the system (3.17) is

$$\bar{h} = 1 - \alpha, \quad \bar{q} = \frac{1}{4}\left[-\ln(\alpha) - \frac{(1 - \alpha^2)(3 - \alpha^2)}{4}\right]. \tag{4.1a,b}$$

The linear stability analysis is implemented by perturbing the base state (4.1) with an infinitesimal harmonic disturbance

$$h = 1 - \alpha + \hat{h}\mathrm{e}^{\mathrm{i}kz + \lambda t}, \tag{4.2}$$

where $\hat{h}$ is the amplitude of the disturbance, k the wavenumber, $\lambda = \lambda_r + \mathrm{i}\lambda_i$ the complex temporal growth rate.

After linearizing, we obtain the dispersive relation:

$$\lambda_r = \frac{k^2}{16}\left[\frac{E_b(1-\ln\beta)}{(\ln\beta)^3} + (1-\epsilon^2 k^2)\right][-4\ln\alpha - (1-\alpha^2)(3-\alpha^2)], \tag{4.3}$$

$$\lambda_i = \frac{k}{2}(2\ln\alpha + 1 - \alpha^2). \tag{4.4}$$

The dispersive relation is identical to that obtained by Craster & Matar (2006) when the electric field is turned off, i.e. $E_b = 0$. The imaginary part of the eigenvalue, λ_i, is independent of the electric field. Therefore, the electric field has no influence on the linear wave speed, but it is questionable as to whether the electric field affects the nonlinear wave speed. A detailed discussion will be presented in § 6. The eigenvalue λ can be connected to ω by $\omega = \epsilon\lambda$ and the wavenumber k can be connected to κ by $\kappa = \epsilon k$ (Craster & Matar 2006). Here, ω and κ are the eigenvalue and wavenumber defined in the appendix. Recall that $\mathscr{E} = E_b/\epsilon$, $\mathscr{S} = 1/\epsilon$. We eliminate ϵ from (4.3) and rewrite the dispersive relation as

$$\omega_r = \frac{\kappa^2}{16}\left[\frac{\mathscr{E}(1-\ln\beta)}{(\ln\beta)^3} + \mathscr{S}(1-\kappa^2)\right][-4\ln\alpha - (1-\alpha^2)(3-\alpha^2)], \tag{4.5}$$

$$\omega_i = \frac{\kappa}{2}(2\ln\alpha + 1 - \alpha^2). \tag{4.6}$$

It is interesting to see that the electric field's influence on the linear stability is dependent on the dimensionless radius β. When κ is very small, i.e. in the long-wave range, if $\beta < e$, the electric field is destabilizing. When $\beta > e$, the electric field is stabilizing. In addition, when $\beta = e$, the electric field has no influence on the long-wave stability. The same conclusion can be obtained from (A 13) in the appendix. In order to explain the physical mechanism clearly, let us refer to figure 2. The perturbed electrical force $\bar{E}q_s'$ is responsible for the interfacial instability. Here $q_s' = -\varepsilon(1-\ln(\beta))/(\ln(\beta)^2)H + O(H^2)$ is the perturbed surface charge density, where H measures the deformation of the interface. The linear stability analysis assumes that H is small such that the terms of order $O(H^2)$ and higher can be neglected. Here $\bar{E}$ is the electric strength at the basic state. Note that the base electric field's always acts in the opposite direction of r. When $\beta < e$, in the elevated region of the interface $q_s' < 0$; while $q_s' > 0$ in the depressed region of the interface. Hence, the electrical force will enhance the deformation of the interface. For $\beta > e$, in the elevated region of the interface $q_s' > 0$; while $q_s' < 0$ in the depressed region of the interface. Hence, the electrical force will impede the deformation of the interface. For $\beta = e$, however, the perturbed charge density $q_s' = 0$. Thereby, the electric field has a negligible influence on the linear stability of the interface.

The numerical results of the fully linearized problem and the dispersive relation (4.5) are shown in figure 3. In the calculation of the fully linearized problem, the Reynolds number is set to be very small so as to study the instability of the Stokes flow (Kliakhandler *et al.* 2001). Two different values of the fibre radius α and three typical values of the outer electrode radius β are investigated. The influence of α is clear when we compare figure 3(*a–c*) with 3(*d–f*) that a smaller α is describing a larger real growth rate ω_r. This phenomenon is due to the surface tension's effect as explained in the work of Ding *et al.* (Ding & Liu 2011; Ding *et al.* 2013) who reported the stability of a liquid film falling down a porous cylinder and indicated that the smaller radius of the cylinder was the more unstable system. Results in figure 3

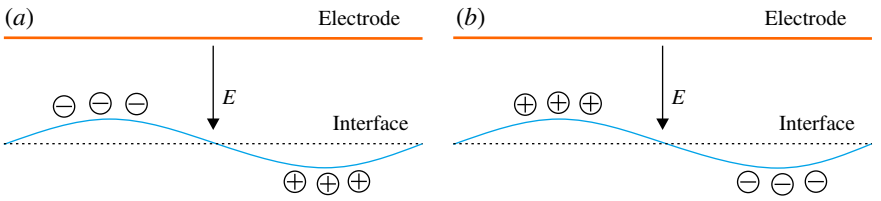

FIGURE 2. (Colour online) The physical mechanism of interfacial instability. Plus/minus symbols stand for positive/negative disturbance charges: (*a*) $\beta < e$; (*b*) $\beta > e$.

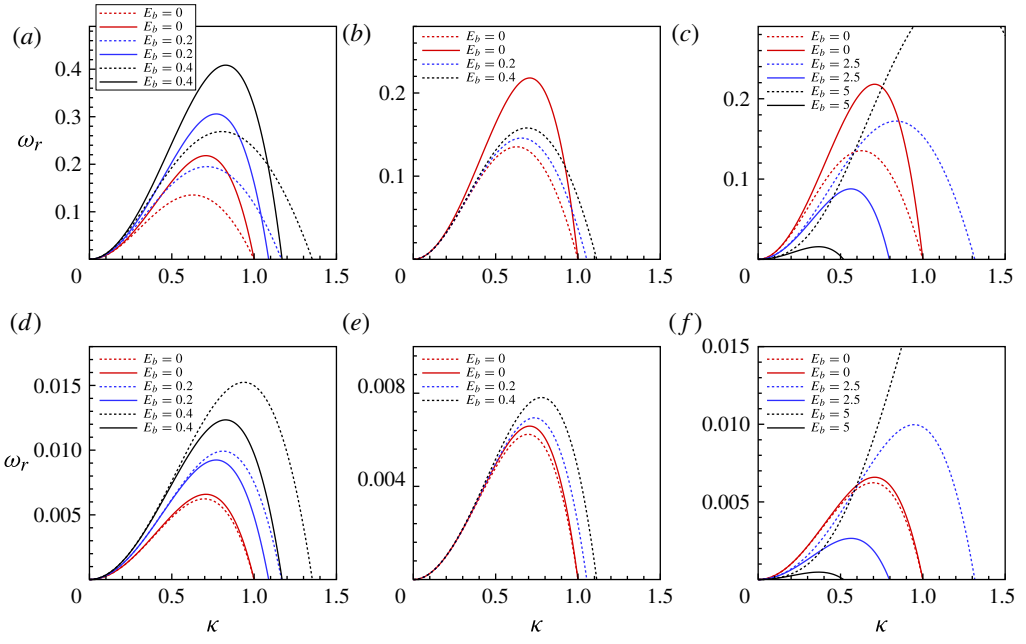

FIGURE 3. (Colour online) The real growth rate ω_r versus the wavenumber κ. Solid lines are obtained by the asymptotic model. Dashed lines are obtained by the fully linearized problem. (*a–c*) The dependent parameters are $\alpha = 0.25$, $\epsilon = 0.2$, $\beta = 2, e, 5$. (*d–f*) The dependent parameters are $\alpha = 0.75$, $\epsilon = 0.2$, $\beta = 2, e, 5$.

show that the asymptotic model does not compare well with the fully linearized problem when α is small. However, in the long-wave range, inspection of the plot reveals that the prediction of asymptotic model agrees well with the fully linearized problem. Craster & Matar (2006) reported that the linear stability result of their asymptotic model compared well with the result of the Stokes flow when $\alpha \geqslant 0.4$; while the agreement deteriorated when α was small. Here, we observe that, when $\alpha > 0.4$, results of the asymptotic model agree well with that of the fully linearized problem when $E_b = 0$. The agreement, however, deteriorates for large E_b values as shown in figure 3(*c*,*f*). This is due to the asymptotic deduction of the Laplace's equation (3.4). In addition, when $\beta = e$, the results by the fully linearized problem show that the electrical field has a negligible influence on the long-wave mode, but destabilizes the short-wave mode. When $\beta = 5 > e$, the electric field tends to stabilize the long-wave mode, while it destabilizes the short-wave mode as shown in

figure 3(*c*,*f*). Therefore, we conclude that, the asymptotic model is valid in the long wave range.

From (4.5), it is found that if

$$\mathscr{S}(1-\kappa^2)+[\mathscr{E}(1-\ln\beta)]/[(\ln\beta)]^3\leqslant 0, \tag{4.7}$$

the long-wave instability can be completely impeded by the electric field. A sufficient condition that the system is stable in the long-wave range can be defined as

$$\mathscr{S}+[\mathscr{E}(1-\ln\beta)]/[(\ln\beta)]^3\leqslant 0. \tag{4.8}$$

We define the maximum real growth rate ω_m of the real growth rate ω_r in (4.5) as

$$\omega_m=\frac{[\mathscr{S}+\mathscr{E}(1-\ln\beta)/(\ln\beta)^3]^2}{64\mathscr{S}}[-4\ln\alpha-(1-\alpha^2)(3-\alpha^2)], \tag{4.9}$$

which occurs at $\kappa_m=\sqrt{1+[\mathscr{E}(1-\ln\beta)]/[\mathscr{S}(\ln\beta)^3]}/\sqrt{2}$ and κ_m is defined as the wavenumber of the most unstable mode (Craster & Matar 2006).

The cut-off wavenumber κ_c corresponding to zero real growth rate is obtained as

$$\kappa_c=\sqrt{1+[\mathscr{E}(1-\ln\beta)]/[\mathscr{S}(\ln\beta)^3]}. \tag{4.10}$$

It is obvious that the cut-off wavenumber varies with the strength of electric field. Both the wavenumbers, κ_m and κ_c are short waves and strictly lie outside the range of validity of the long-wave model. Note that, the wavenumber κ_m and κ_c should be positive and real, which requires $\mathscr{S}+[\mathscr{E}(1-\ln\beta)]/[(\ln\beta)]^3>0$. When $\mathscr{S}+[\mathscr{E}(1-\ln\beta)]/[(\ln\beta)]^3\leqslant 0$, the maximum real growth rate $\omega_m=0$ occurs at $\kappa=0$ and there is no cut-off wavenumber.

When the outer electrode is very close to the liquid interface, i.e. $\beta\to 1$, the maximum real growth rate becomes very large as shown in figure 4(*a*). It indicates that, when $\beta\to 1$, no matter how small the electrical potential difference is, the interfacial instability is enhanced due to the strong attraction between the outer cylinder and the liquid interface. When $\beta\to\infty$, the electric field $\boldsymbol{E}=-\boldsymbol{\nabla}\phi$ vanishes, therefore, the electric field has no influence when β is sufficiently large. This conclusion is useful to explain that a larger β is a more stable system. Our analysis agrees with that of a perfectly conducting liquid jet by Wang *et al.* (2009), which implies that the solid fibre does not change the influence of the electric field on the linear stability of the interface.

From (4.8), we can find a critical electrical Weber number $E_b=(\ln\beta)^3/(\ln\beta-1)$ as shown in figure 4(*b*). Above the value of the critical electrical Weber number, the long-wave instability can be completely impeded. In addition, the smallest value of the critical electrical Weber number $\min(E_b)=27/4$ occurring at $\beta=e^{3/2}$ is found, which is the most economic when we are using an external electric field to impede the long-wave interfacial instability.

5. Nonlinear evolution

This section presents the study of the interface subject to a finite-amplitude harmonic disturbance so as to examine the effect of the electric field on the nonlinear behaviour of the liquid film. We rewrite the evolution equation (3.17) in the conservative form as

$$s_t+(2q)_z=0, \tag{5.1}$$

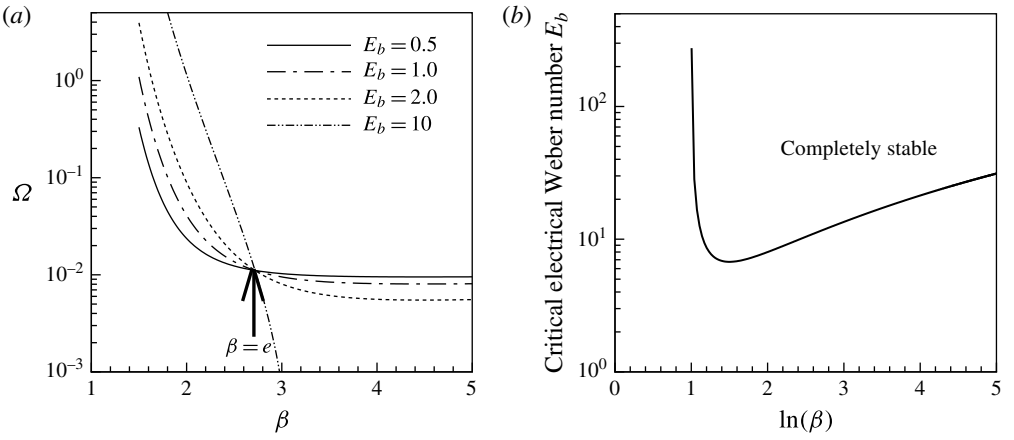

FIGURE 4. (*a*) Plot of $\Omega = \epsilon\omega_m$ versus the radius β predicted by the asymptotic model. (*b*) The electrical Weber number E_b versus the dimensionless radius β predicted by the asymptotic model.

with

$$q = -\frac{p_z - 1}{4}\left[s^2\left(\frac{1}{2}\ln s - \ln\alpha\right) - \frac{\alpha^4 - 4\alpha^2 s + 3s^2}{4}\right], \tag{5.2}$$

where $s = (\alpha + h)^2$ is proportional to the area of a cross-section. The pressure p is modified as

$$p = -\frac{E_b}{2}s^{-1}\left[\frac{1}{2}\ln s - \ln\beta\right]^{-2} + \frac{1}{\sqrt{s}} - \epsilon^2(\sqrt{s})_{zz}. \tag{5.3}$$

The following initial condition is considered that a single harmonic wave is imposed on the interface,

$$s(z, 0) = \left(1 + 0.01\cos\left(\frac{2\pi z}{L}\right)\right)^2. \tag{5.4}$$

Periodical boundary conditions are considered to simulate the nonlinear evolution of the interface. The computational domain is $z = [0, L]$, where L is the length of the domain. The wavenumber $k = 2\pi/L$. In § 4, we have indicated that the asymptotic model is valid in the long-wave range, therefore $\kappa = \epsilon k$ should be small, i.e. L/ϵ should be large. Craster & Matar (2006) proposed that, in spite of the poor agreement in the linear stability analysis between the asymptotic model and the Stokes flow when α is small, the asymptotic model can still be used to study long-wave dynamics of the film. Their numerical study was in excellent agreement with experimental observations (Craster & Matar 2006). In this section, we follow the work of Craster & Matar (2006), and investigate three typical values of $\alpha = 0.26$, 0.28, 0.32 and $\epsilon = 0.29$, 0.23, 0.178 which are close to the experimental values of α and ϵ by Kliakhandler *et al.* (2001).

Before we perform the numerical study, the value of $\sqrt{s}$ should be bounded in (α, β). When the interface touches the surface of the fibre or the outer electrode, we terminate the computation.

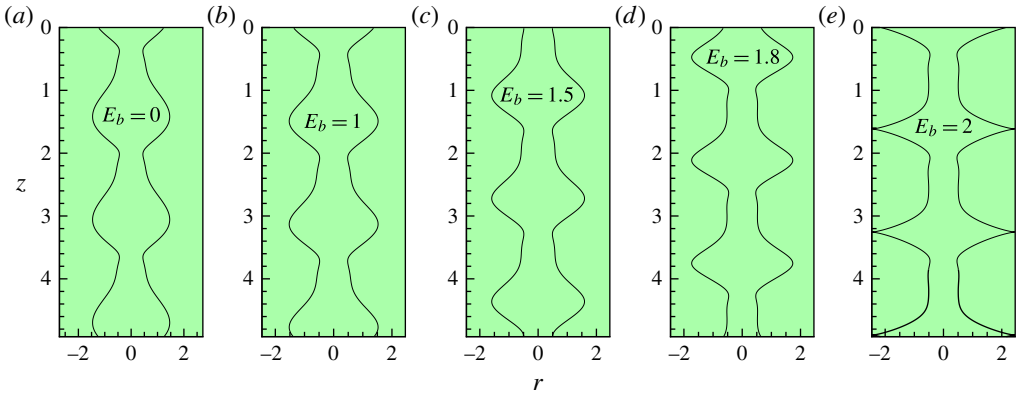

FIGURE 5. (Colour online) (*a–d*) The periodically extended interfacial shape at instant time $t = 100$. (*e*) The periodic extended interfacial shape at instant time $t = 9.10$. The other dependent parameters are $\alpha = 0.28$, $\beta = e^{0.9}$, $\epsilon = 0.23$ and $L = 1.64$.

The solution is approximated by the Fourier series:

$$s(z, t) = \sum_{-N/2}^{N/2} \hat{s}_n(t) \exp(2in\pi/Lz) + \text{c.c}, \tag{5.5}$$

where $\hat{s}_n$ is the time-dependent coefficient and N is the number of Fourier modes. In the present study, 128–512 Fourier modes are enough to provide sufficient accuracy. An implicit Gear's method in time is implemented and the relative error is set less than 10^{-6}.

Figure 5 displays the interfacial shape of the liquid film at instant time for $\beta = e^{0.9}$. According to the linear stability analysis, the electrical field is destabilizing in this case. The values of ϵ and α are fixed at $\epsilon = 0.23$ and $\alpha = 0.28$. The computational length is chosen to be at $L = 1.64$, and thus the wavenumber $\kappa \approx 0.88$. The wavenumber strictly lies outside the range of validity of the long-wave model. However, the flow pattern in figure 5(*a*) is similar to the flow regime 'b' in the experimental observation by Kliakhandler *et al.* (2001). Craster & Matar (2006) used the asymptotic model to investigate the dynamics of such close-spacing droplets and found that this was not in agreement with the experimental observation. However, they still used the asymptotic model to examine the dynamics of such a flow pattern in order to give a complete study of the asymptotic model (Craster & Matar 2006). Similarly, in this paper, it is informative to show how the electric field affects the solution of closely spaced droplets. The results here are also given for completeness, because we are interested in the influence of the electric field on the three typical flow regimes. It is observed that the liquid droplet becomes steeper as E_b increases. When electrical Weber is increased to $E_b = 2$, the liquid interface becomes singular and touches the outer electrode at $t \approx 9.10$ as shown in figure 5(*e*). The maximum value of the radius of liquid film, r_{max}, is plotted against the evolution time t in figure 6(*a*). It is observed that the system can evolve to a steady state after a long time when E_b is less than a certain value. Moreover, the height of the liquid film is promoted by the electric field as shown in figure 6(*a*). In addition, the growth rate of r_{max} is larger for a larger E_b which demonstrates that the instability is enhanced by the electric field. In order to search for the critical value of E_b whereas the liquid film finally touches the outer electrode rather than evolves to a steady state, the

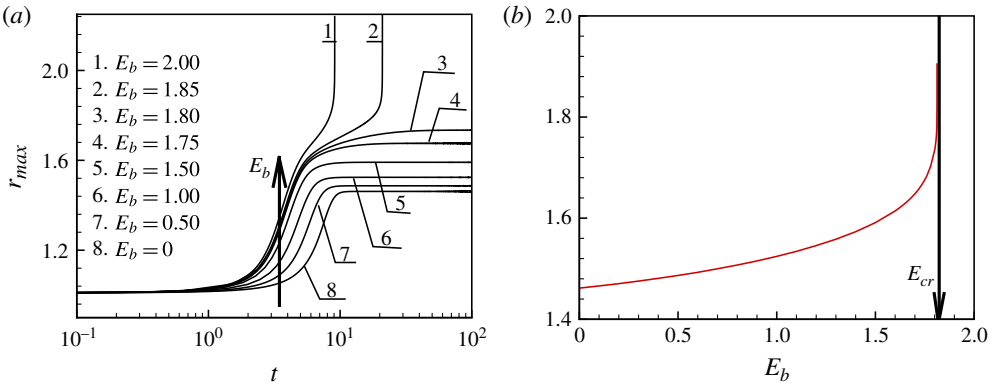

FIGURE 6. (Colour online) (*a*) The maximum radius r_{max} versus the evolution time t. (*b*) The maximum radius r_{max} versus the electrical Weber number. The other dependent parameters are $\alpha = 0.28$ and $\beta = e^{0.9}$. Here $\epsilon = 0.23$ and $L = 1.64$.

numerical simulation is utilized. Here r_{max} is plotted against E_b in figure 6(*b*), in which the critical value of E_b is indicated by $E_{cr} \approx 1.81$. Figure 6(*b*) also shows that the height of the liquid film increases as E_b increases, indicating the electric field is destabilizing. Results in figures 5 and 6 demonstrate that the nonlinear study agrees well with the linear stability analysis that the electric field enhances the instability when $\beta < e$.

The nonlinear behaviour of the liquid film for $\beta = e$ is of particular interest since the linear stability analysis indicates that the electric field has no influence on the long-wave instability. In fact, the liquid film is unstable due to the Plateau–Rayleigh mechanism even when the electric field is switched off. When the liquid film evolves to a new saturated state due to the capillary instability, the gap between the crest of the film and the electrode should be smaller than e. Therefore, in the presence of an electric field, the nonlinear behaviour of the interface should be affected significantly. To study the problem, the conditions $\alpha = 0.26$, $\epsilon = 0.29$ and $L = 5.8$ are chosen. It should be noted that the numerical simulation result relies on the initial condition and we cannot obtain a similar result as Kliakhandler *et al.* (2001) observed in the flow regime 'b'. However, the study in this section can provide insights to explain the effect of the electric field on the nonlinear dynamics of the liquid film. Figure 7(*a*) illustrates the interfacial shape for $E_b = 0$. The influence of the electric field on the interfacial shape is shown in figure 7(*b–e*). An interesting phenomenon observed is that the amplitude of the liquid film starts to oscillate when the electric field is increased to a certain value, for instance $E_b = 2$. In figure 7(*f*), the evolution of r_{max} with time t is shown. It shows that, when the liquid film evolves to a saturated state, the wave amplitude can be either time-independent or time-dependent. The oscillation in the wave amplitude indicates that the state of the film is not steady. To illustrate this phenomenon, we plot the interface shape at different times in figure 7(*g*). The comparison of interfacial wave shape shows that, at the two different times, the distance between the wave crests l_1, l_2 as well as the heights of the wave crests are different. A further increase in the strength of the electric field will cause the liquid film to touch the outer electrode, for instance $E_b = 2.5, 4$.

It is observed that when $E_b = 2.5$, the liquid film touches the outer electrode at $t \approx 64.717$. The simulation of this process is presented in figure 8(*a–c*). To ensure the

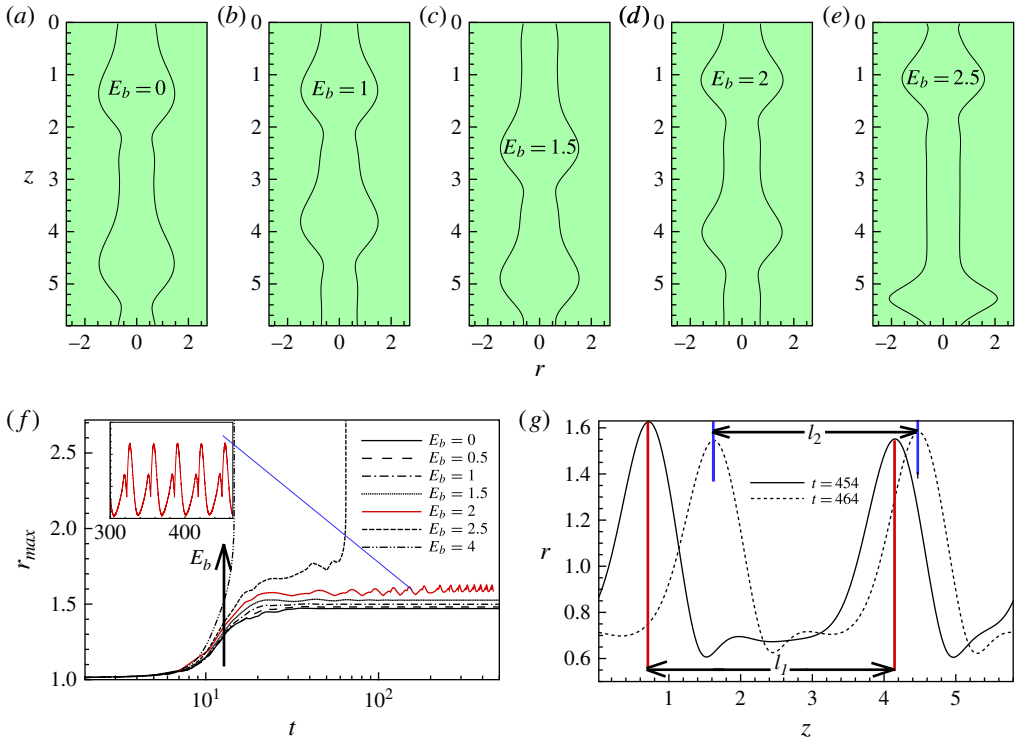

FIGURE 7. (Colour online) (*a–e*) The interfacial shape: (*a–d*) are plotted at $t = 500$; (*e*) is plotted at $t = 64.60$. The other dependent parameters are $\alpha = 0.26$, $\beta = e$, $\epsilon = 0.29$, $L = 5.8$ and $\kappa \approx 0.31$. (*f*) The maximum radius of the liquid ring r_{max} versus the evolution time t. (*g*) The comparison of the interfacial shapes for $E_b = 2$ at different instants of time.

numerical accuracy, we have utilized 512 Fourier modes and the time accuracy for the Gear's method is set less than 10^{-8}. It is observed that the interface becomes singular in a quite short time as seen in figure 8(*a–c*). The electrostatic force is shown in figure 8(*d*). The attraction between the electrode and the liquid interface becomes very large at the crest of the lower droplet, which squeezes the droplet into the singular shape. This phenomenon could also be observed in an electrified jet or thread (Wang *et al.* 2009; Wang & Papageorgiou 2011). Results in figures 7 and 8 indicate that the electric field is destabilizing in the nonlinear regime, but it does not contradict with the linear theory. In figure 7(*f*), the electric field has almost no effect on the evolution of r_{max} in a short time, which implies that the growth rate of the harmonic wave is almost the same. It indicates that, when the deformation of the interface is small, the prediction of linear stability analysis is correct.

When the radius β is increased to $e^{1.1}$, and other parameters used in figure 7 are fixed, the influence of the electric field on the nonlinear behaviour of the interface becomes more complex. The linear stability analysis indicates that the electric field plays a stabilizing role when $\beta > e$. When the nonlinear mechanism becomes important, the electric field can enhance the instability. Clearly, figure 9(*a–e*) shows the flow pattern can be changed by the electrical field. Figure 9(*f*) shows that, when E_b is slightly increased, r_{max} decreases and the liquid film evolves to a steady state. Here r_{max} starts to oscillate when E_b is further increased, for instance

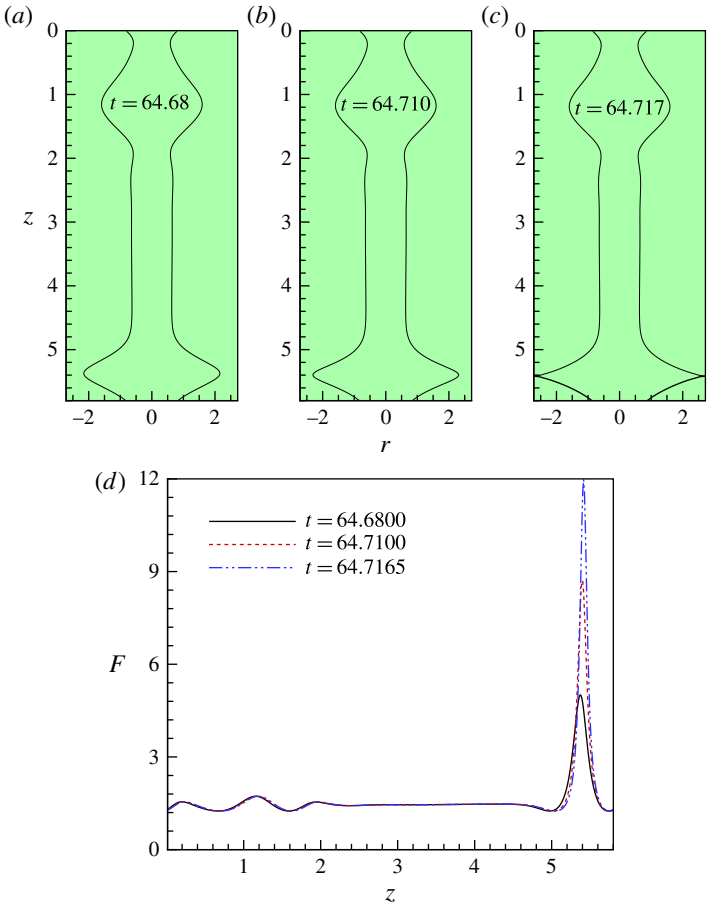

FIGURE 8. (Colour online) (*a–c*) The interfacial shape at different instant time for $E_b = 2.5$. (*d*) The distribution of electrostatic force F at the liquid interface. The other dependent parameters are from figure 7.

$E_b = 1$, 2, 3.7. The transient simulation shows that when $E_b < 3.719$, r_{max} becomes smaller with increasing the value of E_b. However, the oscillation in the amplitude is promoted by the electric field. As the liquid film is not steady, the coalescence event may happen when E_b is further increased. The maximum height of the film will increase due to the coalescence of the droplets. As a result, the gap between the wave crest and the electrode becomes smaller. Thereby, the electrode may attract the interface to its surface. This mechanism can be understood by referring to figure 9(*g*), in which the coalescence of droplets is shown. Numerical simulation have found out that, when $3.719 < E_b < 11.125$, the electric field can attract the liquid film to the outer electrode due to the droplet coalescence. When $E_b > 11.125$, no rupture phenomenon is observed by numerical study and the wave becomes steady after quite a long time ($t > 10^4$). This is due to the electrostatic force which suppresses the deformation of the interface. The wave amplitude is so small that the electric field could not attract the interface to the outer electrode. The liquid film becomes completely stable when $E_b > (\ln \beta)^3(1 - \kappa^2)/(\ln \beta - 1) \approx 12$, which agrees with the linear stability analysis. Aside from that, in figure 9(*f*), it is clear that the growth

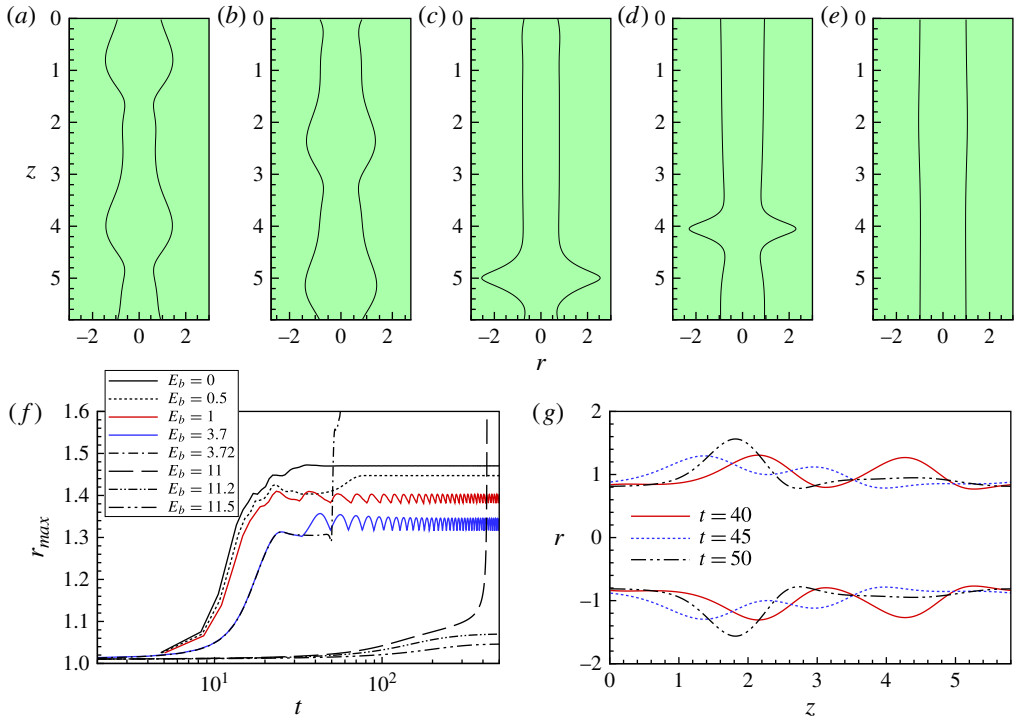

FIGURE 9. (Colour online) (*a–e*) The interfacial shape: (*a*) $E_b = 0.5$, $t = 500$; (*b*) $E_b = 2$, $t = 500$; (*c*) $E_b = 3.72$, $t = 61.83$; (*d*) $E_b = 11$, $t = 423.28$; (*e*) $E_b = 11.5$, $t = 500$. (*f*) The maximum radius of the liquid ring r_{max} versus the evolution time t. (*g*) The comparison of the interfacial shapes for $E_b = 3.72$ at different instants of time. The other dependent parameters are $\alpha = 0.26$, $\beta = e^{1.1}$, $\epsilon = 0.29$, $L = 5.8$ and $\kappa \approx 0.31$.

rate of r_{max} is smaller for a larger E_b for short-time behaviour, which agrees with the linear stability analysis.

Now, we are interested in the case: $\beta = e^{3/2}$. For the chosen value of β, the electric field is stabilizing according to the linear stability analysis. In this case, the values $\alpha = 0.32$, $\epsilon = 0.178$ and $L = 5$ are chosen. A study from Craster & Matar (2006) suggests that a similar flow pattern to flow regime 'c' in the literature (Kliakhandler *et al.* 2001) may be found by transient simulation for a very small ϵ. Meanwhile, the initial condition of the transient simulation was chosen by a travelling wave solution perturbed by pseudo-random noise (Craster & Matar 2006). Moreover, 1024 Fourier modes were used for the numerical simulation (Craster & Matar 2006) which was time-consuming. In this section, we are focusing on the influence of electric field on the stability of the annular liquid film. For convenience, we choose $L = 5$ and use the initial condition (5.4) to explain the influence of electric field. The interfacial shape without the external electric field is shown in figure 10(*a*). When we turn on the electric field, the interfacial wave pattern changes as E_b increases as seen in figure 10(*b–e*). Figure 10(*g*) shows the comparison of the shape of steady wave for $E_b = 5, 5.5$. A clearer figure is shown in figure 10(*f*) that r_{max} becomes smaller as E_b increases. This phenomenon indicates that the electric field is stabilizing. When the electric field is turned on, the permanent wave can also be time-dependent (for instance $E_b = 4$) or time-independent (for instance $E_b = 5$). In this study: $\beta = e^{3/2}$,

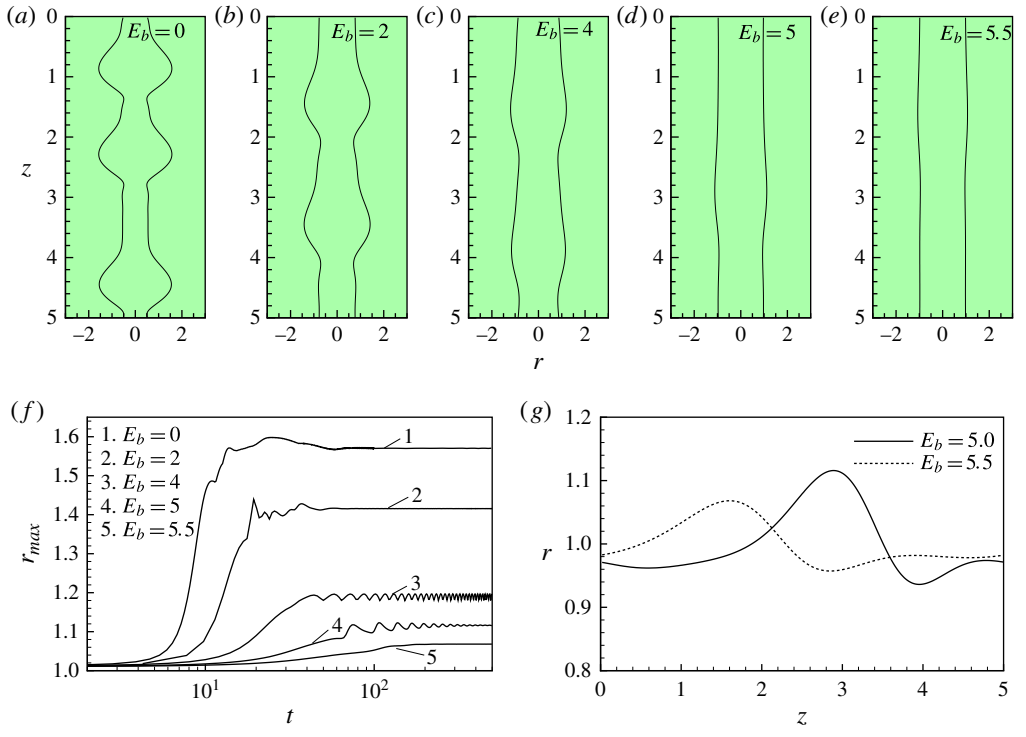

FIGURE 10. (Colour online) (*a–e*) The interfacial shape at $t = 500$. The other dependent parameters are $\alpha = 0.32$, $\beta = e^{3/2}$, $\epsilon = 0.178$, $L = 5$ and $\kappa \approx 0.226$. (*f*) The maximum radius of the liquid ring r_{max} versus the evolution time t. (*g*) The comparison of the interfacial shapes for $E_b = 5, 5.5$.

we do not observe the singular phenomenon for any electrical Weber number $E_b > 0$, which indicates that moving the electrode further from the liquid ring can avoid the singular event that may occur in the system.

Finally, we investigate the transient simulation with a large $L = 20$ so as to understand the complex dynamics of the film. This study is carried out to investigate the response of the liquid film subject to the finite-amplitude wave in a long computational domain. To simulate the problem, we have utilized 512 Fourier modes. The radius of the electrode is fixed at $\beta = e^{1.5}$. We observe that, the film evolves to a steady state for $E_b = 1$ as shown in figure 11(*a*) while it does not become steady for $E_b = 2.5$ as shown in figure 11(*b*). (Note that here the spatial axis is z/ϵ rather than z.) In fact, for $E_b = 2.5$, no steady state was observed for quite a long time, $t = 5000$. The film is oscillating due to the competition between coalescence of droplet and transition to smaller scales (Craster & Matar 2006). To illustrate the phenomenon, the space–time diagram of the liquid film is shown in figure 11(*b*) where the crossing of lines indicate the coalescence of droplets.

6. Travelling wave solution

In § 5, the direct simulation of the asymptotic model has been implemented to study the electric field's influence on the nonlinear behaviour of the liquid film. However, the study could not answer the question: how does the electric field

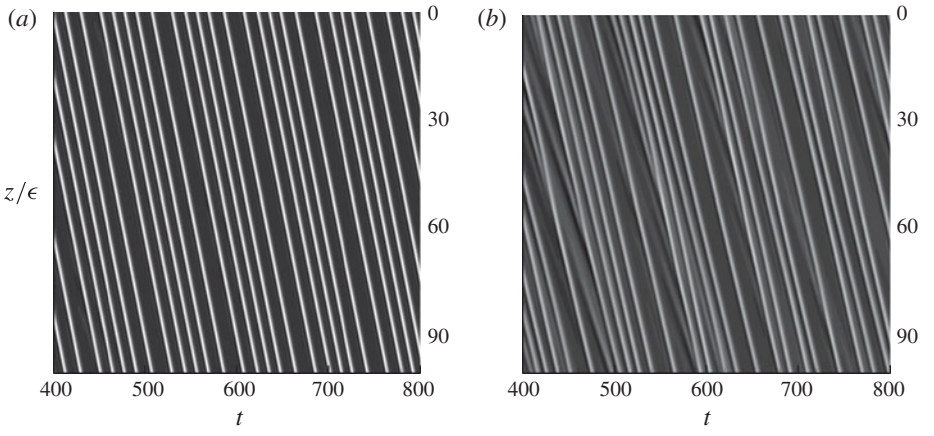

FIGURE 11. Space–time diagram illustrating the dynamics of liquid film, in which the light and dark shading indicate elevated and depressed regions, respectively: (*a*) $E_b = 1$, (*b*) $E_b = 2.5$. The dependent parameters are $\alpha = 0.6$, $\epsilon = 0.2$, $\beta = e^{1.5}$, $L = 20$ and $\kappa \approx 0.0628$.

influence the travelling speed of the steady waves? In this section, we seek travelling wave solutions, i.e. stationary solutions of (5.1) in a frame of reference moving downstream at constant speed c. We introduce the following transformation:

$$\zeta = z - ct. \tag{6.1}$$

Equation (5.1) is then transformed into

$$-cs_\zeta + (2q)_\zeta = 0. \tag{6.2}$$

The unknown variable is set to $s = s(\zeta)$. For a given L (the computational length as defined in § 5), this is a nonlinear eigenvalue problem where s and c are to be determined. The computational length L also corresponds to the droplet–droplet spacing for a single-droplet solution.

Here, we define the flow rate m in the moving frame as

$$m = -\int_{\alpha}^{\alpha+h(\zeta)} r[w(\zeta) - c]\,\mathrm{d}r. \tag{6.3}$$

The solution of s can be approximated by the Fourier series,

$$s(\zeta) = \sum_{-N/2}^{N/2} \hat{s}\mathrm{e}^{2in\pi/L\zeta} + \text{c.c.} \tag{6.4}$$

Since the wave speed c as well as s are unknown, one more condition is needed to fix c. We follow Craster and Matar's work and apply the following condition as a constraint on the fluid mass (Craster & Matar 2006)

$$\frac{1}{L}\int_0^L s\,\mathrm{d}\zeta = 1. \tag{6.5}$$

We begin with a reasonable guess for the wave speed and profile, which via Newton iterations rapidly converges to the solution. A continuation method is used to track the solution branch as parameter changes.

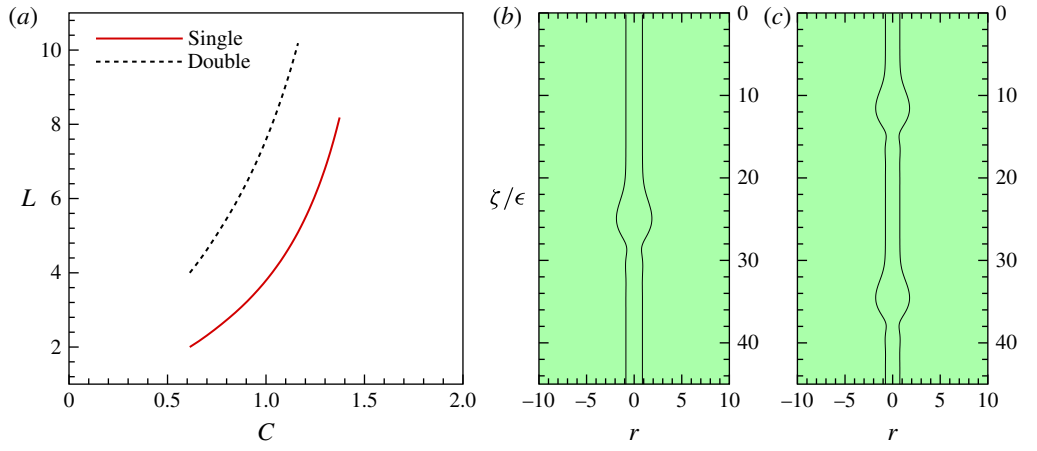

FIGURE 12. (Colour online) (*a*) The wave speed c versus the length L. (*b*) The interfacial shape for a single droplet. Here $c = 1.37$, $L = 8.185$. (*c*) The interfacial shape for two droplets. Here $c = 1.04$, $L = 8.185$, $\alpha = 0.3262$, $\epsilon = 0.178$. 'Single/double' means there is(are) one/two droplet(s) in the computational domain.

It should be indicated that the travelling wave transformation (6.1) is only valid when a travelling wave solution exists. The numerical simulation has indicated that the liquid film may become singular in the presence of an electric field. Therefore, in this situation, there is no steady travelling wave and the solution cannot be found.

First, we revisit the case $\alpha = 0.3262$, $\epsilon = 0.178$, $L = 8.185$ in the work of Craster & Matar (2006). The solution is tracked by the length L. Clearly, a larger L describes a larger wave speed. Figure 12 demonstrates that the asymptotic equation (6.2) exhibits non-uniqueness of solutions. For a given spatial interval, there could have one or two droplets as seen in figure 12(*b*,*c*). Our numerical study gives the wave speed $c = 1.37$ at $L = 8.185$ for a single bead which compares well with the result of Craster and Matar ($c = 1.36$ at $L = 8.185$ for a single bead; see Craster & Matar 2006). This agreement confirms the validity of our numerical method.

Second, we investigate the influence of electric field on these kinds of solutions in figure 12(*b*,*c*). The electrical Weber number is fixed at $E_b = 0.1$ while the radius of the electrode β is varied. Results are shown in figure 13. When $\beta < e$, for instance $\beta = e^{0.9}$, $e^{0.95}$, the travelling wave solution is not found when L exceeds a critical value. When $\beta > e$, the solution does exist. We note that, when $\beta < e$, the electric field promotes the wave speed. When $\beta > e$, the wave speed becomes smaller as β increases.

The influence of the electric field on the travelling waves for $\alpha = 0.28$, $\epsilon = 0.23$, $L = 1.64$ is examined by the asymptotic model. The result of numerical simulation in figure 5(*a*) without periodical extension (a single droplet in the computational domain) is chosen as the initial guess of the wave profile. The results are shown in figure 14. The solution agrees with the numerical simulation as seen in figure 14(*b*). The critical electrical Weber number E_{cr}, above which there is no steady travelling waves, $E_{cr} \approx 1.81$ is re-obtained by the travelling wave study. It is interesting to note that although the height of the wave always increases as E_b increases, the wave speed c starts to decrease at $E_b \approx 1.78$ as observed in figure 14(*a*). The physical mechanism underlying this phenomenon should be the electric field's enhancement on the circulation flow in

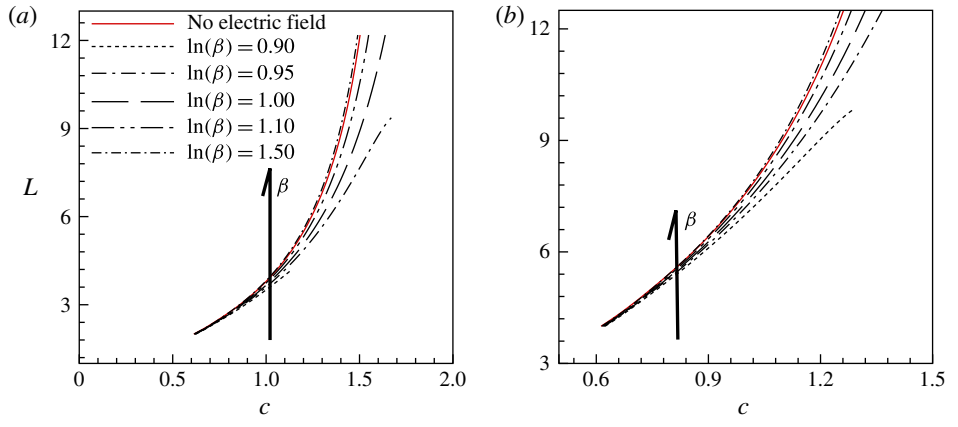

FIGURE 13. (Colour online) (*a*) The wave speed c versus the length L for a single droplet case. (*b*) The wave speed c versus the length L for two droplets case. The dependent parameters are $E_b = 0.1$, $\alpha = 0.3262$ and $\epsilon = 0.178$.

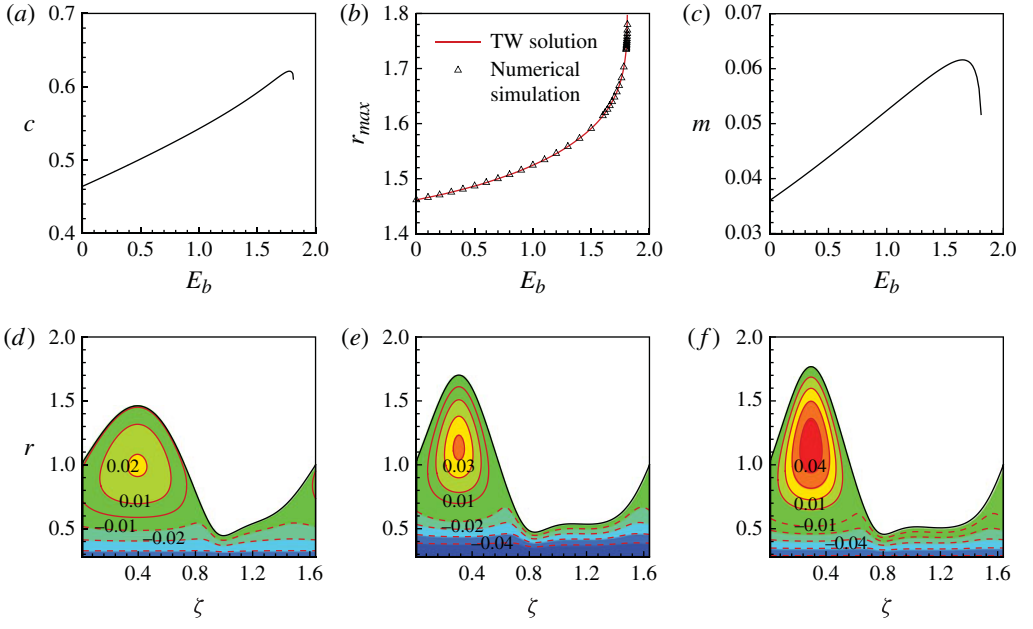

FIGURE 14. (Colour online) (*a*) The wave speed c versus E_b. (*b*) The maximum height r_{max} versus E_b, in which 'TW' stands for travelling wave. (*c*) The flow rate m in the moving frame versus E_b. (*d–f*) Streamlines in the moving frame with constant speed c, in which $E_b = 0$, 1.78, 1.81, respectively. The dependent parameters are $\alpha = 0.28$, $\beta = e^{0.9}$, $\epsilon = 0.23$ and $L = 1.64$.

the wave crest (see figure 14*d–f*). The flow rate m increases as E_b increases until $E_b \approx 1.78$, indicating that the electric field enhances the flow, therefore, a larger c. However, the circulation in the wave crest may retard the flow as $E_b > 1.78$, therefore causing the flow rate m to become smaller. Thereby, the wave speed may become smaller due to the decrease of flow rate.

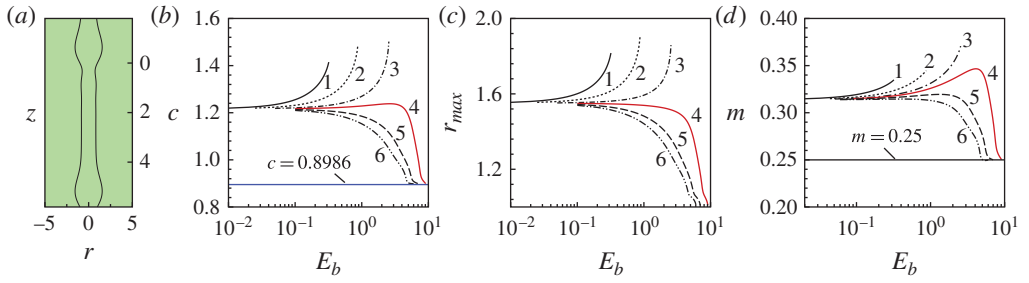

FIGURE 15. (Colour online) (*a*) The wave profile for $E_b = 0$. (*b*) The wave speed c versus the electrical Weber number E_b. (*c*) The maximum height r_{max} versus the electrical Weber number E_b. (*d*) The flow rate m versus E_b. The marked lines: '1' $\ln(\beta) = 0.9$; '2' $\ln(\beta) = 1$; '3' $\ln(\beta) = 1.1$; '4' $\ln(\beta) = 1.15$; '5' $\ln(\beta) = 1.25$; '6' $\ln(\beta) = 1.5$. The other dependent parameters are $\alpha = 0.2551$, $\epsilon = 0.2915$ and $L = 5.81$.

The influence of the electrical field on the travelling waves for $\alpha = 0.2551$, $\epsilon = 0.2915$ and $L = 5.81$ (α, ϵ and L are the experimental values of flow regime 'a'; see Kliakhandler *et al.* 2001) is investigated here. For non-zero E_b, the solution is tracked by the parameter E_b. The wave speed for $E_b = 0$ is $c = 1.21$, which agrees well with Craster and Matar's study (Craster & Matar (2006) gave $c = 1.195$). Influences of the electric field on the wave speed c and the maximum height r_{max} as well as the flow rate m are shown in figure 15(*b–d*). Numerical results indicate that (c, r_{max}, m) increase with E_b when $\ln\beta < 1.1$. When $\ln\beta = 1.15$, we observe an interesting phenomenon that, although r_{max} decreases with E_b, c and m reach to their maximum values after that they start to decrease. This phenomenon implies that the electric field enhances the flow and promotes the wave speed. When $\ln\beta > 1.2$, c and r_{max} are observed to decrease as E_b increases. It is found that, for $\ln\beta = 1.15$, 1.25, 1.5, $r_{max} \to 1$, $c \to 0.8986$, $m \to 0.25$ as E_b increases to $E_b \approx 9.1$, 7, 6, respectively. The constant value $c = 0.8986$ is nothing but the linear wave speed $c_l = -(\omega_i/\kappa) = -(2\ln\alpha + 1 - \alpha^2)/2$. The flow rate $m = 0.25$ is the basic flow rate in the moving frame with the constant speed c_l: $m = c_l(1 - \alpha^2) - \bar{q}$. The critical electrical Weber number $E_b = (\ln\beta)^3(1 - \kappa^2)/(\ln\beta - 1)$ predicted by the linear stability theory gives $E_b \approx 9.13$, 7.03, 6.07 for the three cases: $\ln\beta = 1.15$, 1.25, 1.5, which agrees with the study of the travelling waves.

7. Conclusion

In this paper, we have investigated the long-wave dynamics of perfectly conducting viscous liquid films on a vertical fibre in the presence of a radial electric field. An asymptotic model was derived to study the linear and nonlinear dynamics of the film. The validity of the asymptotic model was verified by the fully linearized Navier–Stokes equations.

Linear stability analysis of the asymptotic model indicated that, when the ratio between radius of the outer electrode and the initial radius of the liquid film $\beta < e$, the linear instability was enhanced by the electric field; when $\beta = e$, the electric field had a negligible influence on the linear instability; when $\beta > e$, the electric field impeded the linear instability. Nonlinear simulation of the asymptotic model was studied. When $\beta < e$, the electric field promoted the wave height, which can cause the film to be singular. When $\beta = e$, the nonlinear simulation showed that

the electric field enhanced the deformation of the interface. When $\beta \geqslant e$, the study showed that the permanent wave may be time-dependent or time-independent which was dependent on the strength of the electric field. For instance, when $\beta = e^{1.1}$, the electric field can lead to the droplet coalescence and therefore cause the liquid film to be singular. In the study of the case $\beta = e^{1.5}$, we did not observe the singular phenomenon for all electrical Weber number, and the maximum height of the wave decreased as the electrical Weber number increased. Investigation on steady travelling waves was further conducted to discuss the influence of electric field on the wave speed. It was found that the wave speed and the wave amplitude can be promoted or decreased by the electric field. In particular, in some situations, the wave speed may increase/decrease while its amplitude decreased/increased as the strength of the external electric field increased.

Acknowledgements

Z.D. and T.N.W. acknowledge support from Singapore Ministry of Education, Academic Research Fund Tier 2 research grant MOE2011-T2-1-036. The authors acknowledge the referees for their many helpful suggestions and comments. Z. Ding also thanks S. Bindumadhav for his suggestions.

Appendix A. The fully linearized problem

Here, the fully linearized system is carried out so as to verify the validity of the asymptotic model (3.17). The system is non-dimensionalized by using the length scale $\mathscr{R} = a + h_0$, and pressure scale $\rho g \mathscr{R}$, velocity scale $\rho \mathscr{R}^2 g/\mu$, time scale $\mu/\rho \mathscr{R} g$ and electrical potential scale $\phi = \Delta\phi = \phi_0$.

The velocity field $\boldsymbol{u}$, pressure p, the electrical potential ϕ as well as the interface h are perturbed by infinitesimal harmonic disturbances as

$$[u, w, p, \phi, h] = [\bar{u}, \bar{w}, \bar{p}, \bar{\phi}, \bar{h}] + [\hat{u}, \hat{w}, \hat{p}, \hat{\phi}, \hat{h}] \exp(\mathrm{i}\kappa z + \omega t), \tag{A 1}$$

where $\bar{u}$, $\bar{w}$, $\bar{p}$, $\bar{\phi}$, $\bar{h}$ refer to the base state and $\hat{u}$, $\hat{w}$, $\hat{p}$, $\hat{\phi}$, $\hat{h}$ are the Fourier amplitudes of the disturbances. Here κ is the disturbance wavenumber, and ω is the complex temporal growth rate.

The governing equations of the perturbed system are

$$\mathrm{D}\hat{u} + \frac{\hat{u}}{r} + \mathrm{i}\kappa\hat{w} = 0, \tag{A 2}$$

$$\omega\mathcal{R}\hat{u} = -\mathrm{D}\hat{p} + \left(\mathrm{D}^2 + \frac{\mathrm{D}}{r} - \kappa^2\right)\hat{u} - \frac{\hat{u}}{r^2} - \mathrm{i}\kappa\mathcal{R}\bar{w}\hat{u}, \tag{A 3}$$

$$\omega\mathcal{R}\hat{w} = -\mathrm{i}\kappa\hat{p} + \left(\mathrm{D}^2 + \frac{\mathrm{D}}{r} - \kappa^2\right)\hat{w} - \mathcal{R}(\mathrm{i}\kappa\bar{w}\hat{w} + \bar{w}_r\hat{u}), \tag{A 4}$$

$$\left(\mathrm{D}^2 + \frac{\mathrm{D}}{r} - \kappa^2\right)\hat{\phi} = 0, \tag{A 5}$$

in which $\mathrm{D} = \mathrm{d}/\mathrm{d}r$. Here $\mathcal{R} = \rho^2 g \mathcal{R}^3/\mu^2$ can be connected to the Reynolds number by $\mathcal{R} = \epsilon Re$.

The linearized boundary conditions at $r = \alpha$ are

$$\hat{u} = \hat{w} = 0. \tag{A 6}$$

At the liquid interface, the boundary conditions are projected to $r = 1$ by Taylor's expansion,

$$\mathrm{i}\kappa\hat{u} + \mathrm{D}\hat{w} + \mathrm{D}^2\bar{w}\hat{h} = 0, \tag{A 7}$$

$$\hat{p} + 2(\mathrm{i}\kappa\mathrm{D}\bar{w}\hat{h} - \mathrm{D}\hat{u}) + \mathscr{E}\mathrm{D}\bar{\phi}(\mathrm{D}^2\bar{\phi}\hat{h} + \mathrm{D}\hat{\phi}) = \mathscr{S}(\kappa^2 - 1)\hat{h}, \tag{A 8}$$

$$\hat{\phi} + \mathrm{D}\bar{\phi}\hat{h} = 0, \tag{A 9}$$

$$\omega\hat{h} + \mathrm{i}\kappa\bar{w}\hat{h} = \hat{u}. \tag{A 10}$$

Here, the electrical Weber number $\mathscr{E}$ and dimensionless surface tension $\mathscr{S}$ can be connected to the modified dimensionless parameters by $\mathscr{E} = E_b/\epsilon$, $\mathscr{S} = 1/\epsilon$.

At the outer electrode $r = \beta$, the boundary condition for the perturbed electrical potential is

$$\hat{\phi} = 0. \tag{A 11}$$

The perturbed electrical potential is obtained as follows

$$\hat{\phi} = \frac{\hat{h}}{\ln\beta}\frac{I_0(\kappa r)K_0(k\beta) - I_0(\kappa\beta)K_0(\kappa r)}{I_0(\kappa\beta)K_0(\kappa) - I_0(\kappa)K_0(\kappa\beta)}, \tag{A 12}$$

where I_0 and K_0 are the zero-order modified Bessel functions.

In the linearized normal stress balance condition (A 8), the electrical force term reads

$$\frac{\mathscr{E}}{(\ln\beta)^2}\left[-1 + \kappa\frac{I_1(\kappa)K_0(\kappa\beta) + I_0(\kappa\beta)K_1(\kappa)}{I_0(\kappa\beta)K_0(\kappa) - I_0(\kappa)K_0(\kappa\beta)}\right]\hat{h}, \tag{A 13}$$

where I_1 and K_1 are the first-order modified Bessel functions. In the long-wave range, $\kappa \to 0$, the asymptotic electrical force term can be written

$$\frac{\mathscr{E}(1 - \ln\beta)}{(\ln\beta)^3}\hat{h} + O(\kappa^2). \tag{A 14}$$

The above fully linearized problem is solved by a Chebyshev collocation method.

REFERENCES

Basset, A. 1894 Waves and jets in a viscous liquid. *Am. J. Maths* **16**, 93–110.

Collins, R., Harris, M. & Basaran, O. 2007 Breakup of electrified jets. *J. Fluid Mech.* **588**, 75–129.

Conroy, D., Matar, O., Craster, R. & Papageorgiou, D. 2011 Breakup of an electrified perfectly conducting, viscous thread in an AC field. *Phys. Rev.* E **83**, 066314.

Craster, R. & Matar, O. 2006 On viscous beads flowing down a vertical fibre. *J. Fluid Mech.* **553**, 85–105.

De Ryck, A. & Quéré, D. 1996 Inertial coating of a fiber. *J. Fluid Mech.* **311**, 219–237.

Ding, Z. & Liu, Q. 2011 Stability of liquid films on a porous vertical cylinder. *Phys. Rev.* E **84**, 046307.

Ding, Z., Wong, T., Liu, R. & Liu, Q. 2013 Viscous liquid films on a porous vertical cylinder: dynamics and stability. *Phys. Fluids* **25**, 064101.

Duprat, C., Ruyer-Quil, C. & Giorgiutti-Dauphiné, F. 2009 Experimental study of the instability of a film flowing down a vertical fiber. *Eur. Phys. J. Spec. Top.* **166**, 63–66.

Frenkel, A. 1992 Nonlinear thoery of strongly undulating thin films flowing down vertical cylinders. *Europhys. Lett.* **18**, 583–588.

GOREN, S. 1962 The instability of an annular thread of liquid. *J. Fluid Mech.* **12**, 309–319.

KLIAKHANDLER, I., DAVIS, S. & BANKHOFF, S. 2001 Viscous beads on vertical fibre. *J. Fluid Mech.* **429**, 381–390.

LIN, S. P. & LIU, W. C. 1975 Instability of film coating of wires and tubes. *AIChE J.* **21**, 775–782.

LISTER, J., RALLISON, J., KING, A., CUMMINGS, L. & JENSEN, O. 2006 Capillary drainage of an annular film: the dynamics of collars and lobes. *J. Fluid Mech.* **552**, 311–343.

LÓPEZ-HERRERA, J., RIESCO-CHUECA, P. & GAÑÓN-CALVO, A. 2005 Linear stability analysis of axisymmetric perturbations in imperfectly conducting liquid jets. *Phys. Fluids* **17**, 034106.

PUMIR, A., MANNEVILLE, P. & POMEAU, Y. 1983 On solitary waves running down an inclined plane. *J. Fluid Mech.* **135**, 27–50.

QUÉRÉ, D. 1990 Thin-films flowing on vertical fibers. *Europhys. Lett.* **13**, 721–726.

QUÉRÉ, D. 1999 Fluid coating on a fiber. *Annu. Rev. Fluid Mech.* **31**, 347–384.

RUYER-QUIL, C. & KALLIADASIS, S. 2012 Wavy regimes of film flow down a fiber. *Phys. Rev.* E **85**, 046302.

RUYER-QUIL, C. & MANNEVILLE, P. 1998 Modeling Film flows down inclined planes. *Eur. Phys. J.* B **6**, 277–292.

RUYER-QUIL, C., TREVELEYAN, P., GIORGIUTTI-DAUPHINÉ, F. & KALLIADASIS, S. 2008 Modeling film flows down a fibre. *J. Fluid Mech.* **603**, 431–462.

SAVILLE, D. 1971 Stability of electrically charged viscous cylinders. *Phys. Fluids* **14**, 1095–1099.

SHKADOV, V. YA., BELOGLAZKIN, A. & GERASIMOV, S. 2008 Solitary waves in a viscous liquid film flowing down a thin vertical cylinder. *Moscow Univ. Mech. Bull.* **63**, 122–128.

SISOEV, G., CRASTER, R., MATAR, O. & GERASIMOV, S. 2006 Film flow down a fibre at moderate flow rates. *Chem. Engng Sci.* **61**, 7279–7298.

SON, P. & OHBA, K. 1998 Instability of a perfectly conducting liquid jet in electrohydrodynamic spraying: perturbation analysis and experimental verification. *J. Phys. Soc. Japan* **67**, 825–832.

TAYLOR, G. 1969 Electrically driven jets. *Proc. R. Soc. Lond.* A **313**, 453–475.

TRIFONOV, YU. YA. 1992 Steady-state traveling waves on the surface of a viscous liquid film falling down on vertical wires and tubes. *AIChE J.* **38**, 821–834.

WANG, Q. 2012 Breakup of a poorly conducting liquid thread subject to a radial electric field at zero Reynolds number. *Phys. Fluids* **24**, 102102.

WANG, Q., MÄHLMANN, S. & PAPAGEORGIOU, D. 2009 Dynamics of liquid jets and threads under the action of radial electric fields: microthread formation and touchdown singularities. *Phys. Fluids* **21**, 032109.

WANG, Q. & PAPAGEORGIOU, D. 2011 Dynamics of a viscous thread surrounded by another viscous fluid in a cylindrical tube under the action of a radial electric field: breakup and touchdown singularities. *J. Fluid Mech.* **683**, 27–56.

WRAY, A., MATAR, O. & PAPAGEORGIOU, D. 2012 Nonlinear waves in electrified viscous film flow down a vertical cylinder. *IMA J. Appl. Maths* **77**, 430–440.

ZUCCHER, S. 2008 Experimental investigations of the liquid-film instabilities forming on a wire under the action of a die. *Intl J. Heat Fluid Flow* **29**, 1586–1592.